International Journal of
INTELLIGENT SYSTEMS AND APPLICATIONS IN ENGINEERING
ISSN:2147-6799 www.ijisae.org Original Research Paper

Broadband MIMO Configuration Using a Novel Split Ring Metasurface as Superstrate for Gain Enhancement Operating in Millimeter Wave Regime

Vijay Kumar Sahu [1], Dr. Rajyalakshmi Valluri [2], Dr. P. V. Sridevi [3]

Submitted: 03/02/2024 **Revised**: 13/03/2024 **Accepted**: 21/03/2024

Abstract: This paper outlines the design and analysis of a compact antenna and its multiple-input multiple-output (MIMO) arrangement for use in applications at millimetre wave (mmW). The antenna was constructed with the Rogers substrate RT Durioid 5880, which possesses a total dimension of 44 × 44 mm2 with a height of 1.575 mm. The Coplanar Waveguide Fed (CPW) antenna was originally intended to function within a 30 GHz – 50 GHz frequency spectrum. Subsequently, the MIMO configuration of the same antenna is designed and developed over which a metamaterial superstrate was positioned in the design. The proposed MIMO configuration offers a good impedance match over a wide frequency range, considerable gain, minimal coupling among the antennas, and a low ECC, in addition to attaining a high diversity gain. To further highlight the importance of the suggested work, a comparison with related studies has been established.

Keywords: *Compact, Coplanar Waveguide Fed (CPW), high gain, MIMO, Mutual Coupling.*

1. Introduction

The upsurge in the number of annual data traffic, propelled by the rise in wireless devices per user, necessitates high-speed data transport and less delay. The difficulty is further complicated by the increased intricacies encountered by modern wireless communication networks as a result of the growing need for smaller devices [1]. Furthermore, the existing frequency band spectrum is under pressure due to the concurrent application of several technologies superimposed in frequency bands [2]. As a result, the existing wireless technology and spectrum are inadequate to fulfil contemporary requirements [3]. Consequently, researchers are looking into emerging technologies like 5G and, more precisely, the mmW frequency spectrum, which ranges from 30 to 300 GHz. They see this as a possible answer to the rising issues, particularly in the field of millimetre wave applications [4]. The expensive 5G spectrum is particularly significant within the range of frequencies that could be assigned for future millimetre-wave applications because of its pros, like the availability of large bandwidth that enhances the capacity and data rate of the wireless communication system and also offers cons like a high rate of absorption, multipath fading and interference effect due to different channels [5,6]. Moreover, the antenna, which is an essential part of any communication system, requires meticulous planning to tackle the issues outlined above accurately [7]. To address the issues related to absorption, antennas with high gain and low profiles are preferred. Spatial diversity techniques are very helpful in overcoming the effects related to fading and interference of signals. Hence, the MIMO antenna seems to fit as an efficient solution by overcoming the aforementioned problems and establishing a reliable wireless link at the mmW band. Consequently, the academic and research communities are putting tremendous effort into unique types of antennas intended exclusively for millimetre-wave applications like cellphones, electronic gadgets, dongles, smartwatches, and others [8-30].

Millimetre waves are highly prone to attenuation along with absorption by the atmosphere and, hence, are preferred for only short-distance communication. Antennas with high gain and good spatial coverage are the best solution to overcome the problem. Researchers have devised several strategies to address the problem mentioned above in [8-15]. To augment the gain, the MIMO configuration with four antennas constituting a two-element array with corporate feed is presented in [8]. The device operates within the frequencies 25.5 and 29.5 GHz and has an apex gain of 8.3 dBi, which makes it ideal for mmW applications. However, due to the feeding provided, the array induces more losses with the increased number of elements introduced into the array. An asymmetric-fed DRA using slot coupling centred by EBG structures that operate around 60 GHz is presented [9]. This antenna offers a maximum of 8.6 dBi gain with a boost of up to 3.2 dBi throughout the recommended bandwidth while also suppressing the power in the backside direction. A circularly polarized high gain DRA exited with

[1] *Research Scholar Department of Electronics and Communication Engineering Andra University College of Engineering, Andhra University Visakhapatnam-530017. vijaykumarsahu.86@gmail.com*
[2] *Professor Department of Electronics and Communication Engineering Anil Neerukonda Institute of Technology & Sciences (ANITS) Visakhapatnam-531162. rajyalakshmi.ece@anit.edu.in*
[3] *Professor Department of Electronics and Communication Engineering AU College of Engineering, Andhra University Visakhapatnam-530017. pvsridevi1965@gmail.com*

an X- shaped aperture etched in the ground plane is suggested in [10] for application in mmW. A superstrate layer consisting of the frequency-selective surface is used to enhance gain. A patch antenna placed on the surface of a dielectric lens is presented in [11]. The antenna adopts a proximity-coupled technique for excitation and offers a bandwidth of around 8% and a high gain across the frequency range. A slotted array in SIW and a patch array with a partially infilled dielectric lens for different cases in wireless communication applications at mmW frequencies are proposed by the researchers [12]. The designed antenna achieves the maximum gain of 15.6 dBi and a fractional bandwidth of 10.7% for the operating frequency spectrum of 26.5 to 29.4GHz. A two-layered unit cell, with different dimensions on either side consisting of a square-shaped slot in which a grid of the same shape embedded inside constituted to frame an FSS superstrate layer. [13] over a mmW antenna that operates in a V-band with a bandwidth of 20 GHz. It combines a Fabry-Perot Cavity along with the printed ridge gap waveguide to enhance the radiation characteristics. [14] presents a dipole antenna array in MIMO configuration functioning at 28 GHz. The antenna along with capacitive loops loaded make it compact, leading to a complex geometry. However, it proposes a straightforward design with characteristics like high gain and wider bandwidth. A patch antenna made of a dense dielectric excited through an aperture-coupled feeding is proposed in [15]. A reflective type FSS superstrate layer printed on both sides to increase the gain of the antenna. While exhibiting strong radiation characteristics, the impedance bandwidth also enlarged due to the installation of the superstrate layer. Here, even if the antennas are providing the high gain they are still the same single element. Since MIMO technology allows several antennas to function simultaneously, enhancing the capacity, stability and data rate of the communication link, it is seen to be of major significance in increasing the scope of the communication system.

MIMO systems have multiple antennas where isolating one antenna from another is an important design task which if not considered seriously leads to an escalation in the mutual coupling and degrades the performance antenna. When engineered properly with utmost care to reduce, it then enhances the capacity of transmission along with stable radiation all along its operational bands, while in transmitting mode. Various isolation enhancement techniques were developed by several researchers for an antenna in a MIMO system [16-25]. A four-port MIMO system with crossed dipoles as the radiating element was proposed in [16]. Incorporating two layered transmission type FSS over the MIMO arrangement leads to enhancement of isolation among the antenna ports. [17] presents a MIMO configuration with a rectangular Dielectric resonator antenna (DRA). Because of the strong coupling between the resonators, a narrow bandwidth of 2.23 GHz is obtained that spans the FCC-allotted 28GHz band meant for 5G applications. Metamaterial structures were employed to enhance the effect of isolation and claim a gain of about 7dBi in the specified band. To reduce the coupling among the DRA in the MIMO configuration functioning at 57 GHz to 64 GHz band, a metamaterial was engineered [18], that acts as a polarization rotator wall. This Metamaterial Polarization Rotator wall changes the orientation of the field coupled up on it without affecting the properties of the radiation pattern. Using this technique, there is about a 16dB reduction in the mutual coupling. A bow tie antenna integrated with three pairs of High refractive index metamaterial (HRIMTM) is presented in [19]. Here a pair of HRIMTM is used to produce a broad beam while the other two pairs are used to produce a dual beam with high directivity and radiating along the axis. It has a stable pattern and offers a gain of 7.41 dBi functioning in the frequency spectrum of 24.25-27.5GHz. In their study, researchers in [20] suggest a pioneering approach to address coupling between the antennas in MIMO configuration through a unique design of an Electromagnetic Band Gap (EBG) cell. The article presents a broadband antenna in MIMO arrangement that functions at mmW frequencies. In [21], a MIMO antenna appropriate for wearable applications with a simple shape, working at 24 GHz ISM band, was proposed. The antenna setup was fabricated on a flexible substrate and tested for its performance while bending in different ways both on the phantom and free space. The antennas are located close to each other edge to edge and still obtain an enhancement of gain by 1.9dBi due to the array of EBG structure placed behind the radiating patch. The antenna demonstrates improved return loss and a broad frequency range by incorporating a Defected Ground Structure (DGS) [22]. Significantly, it helps to improve the separation among the MIMO antenna, therefore decreasing the Electromagnetic Compatibility (EMC) difficulties [23,26**]**. In addition, a multilayered compact antenna with wideband characteristics is suggested for mobile applications operating at a frequency of 6 GHz and with a bandwidth ranging from 4.5 GHz to 8.5 GHz [24]. A MIMO antenna system with two arrays placed opposite to each other excited with proximity coupled wide slot is presented in [25]. Here, each array consists of three antennas operating in Ka-band. A wider bandwidth of nearly 27 GHz and a realized gain of 11.5 dBi is attained by placing the reflector of the EBG cell behind the structure of the antenna towards the feed. This also helped in enhancing the F/B ratio with a realized gain of 11.5. From studies conducted, as mentioned above, researchers either focus on improving the isolation or increasing the gain of the antenna. That being said, for an antenna to work efficiently, both of these parameters are to be focused especially for designing antennas at mmWaves.

This manuscript introduces a compact broadband antenna designed for millimetre wave applications. Here, the CPW-fed antenna constitutes the base element for the MIMO configuration. The MIMO configuration is made next, after which the metasurface superstrate is designed and loaded for gain enhancement. Sections 2 and 3 provide an in-depth study of the design and analysis of the single antenna, while Sections 4 and 5 expound upon specifics of the MIMO Configuration, and Section 6 explains the MIMO antenna for its diversity performance. Eventually, the discussion is brought to an end by an extensive comparison of the present work with the antennas of cutting technology documented in the existing literature.

2. Design Procedure of Proposed Antenna

The proposed structure of the designed antenna is presented in Fig. 1. The top-side aspect of the antenna schematic is delineated in Fig. 1(a). A CPW Fed antenna is initially designed in the simulator with a feed of dimension $L_Y \times W_Y$. This is followed by the design of the ground plane, which resembles the shape of a stair on both sides of the feeding. Here, S_1, to S_6 are the lengths of each step, while S_h represents the step height within the ground. Once this is designed, the radiating patch on the top side of the substrate is designed appropriately, as depicted above. The top patch also features a staircase-type profile with dimensions varying from F_1 to F_6. The gap between the steps is maintained to be F_h.

Two curves of dimensions F_c are also cut out from the top patch. After this, a circle of diameter F_7 is etched out from the centre of the patch. Finally, a small rectangular notch of dimension $F_8 \times F_9$ is etched out from the top and bottom of the circle along the longitudinal axis to complete the design on the substrate front side. A small incision of length F_d is also made in the ground plane, as illustrated in Fig. 1 (a). Fig. 1 (b) depicts the backside view of the designed structure. In this portion, a circular ring with a split in the shape of the rectangle is designed. Initially, a circular disc of F10 diameter is designed, and another disc of a smaller diameter F_{11} is etched out to result in a circular ring. The split in the circular ring is then designed by etching out a rectangular portion of dimension $F_{12} \times F_{13}$, and so the final structure is achieved. The ring is positioned in such a way that it enhances the performance in terms of matching at the low-frequency range. The profile of the antenna inside view is illustrated in Fig. 1. (c). The substrate RT/Duroid 5880, having an electric permittivity of ε_r=2.2 and a sheet width of 1.575 mm, is used to develop the antenna. The complete collection of physical parameters of the antenna designed and simulated is listed in Table I.

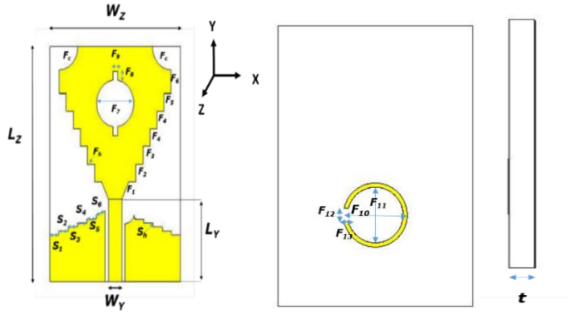

(a) (b) (c)

Fig. 1. Schematic of the proposed antenna. (a) top view (b) back view (c) side view.

Table 1: Proposed Antenna Dimensions in mm

L_Z	W_Z	L_Y	W_Y	S_1
20	14	7	1.5	1
S_2	S_3	S_4	S_5	S_6
1	1	1	1	1
S_h	F_1	F_2	F_3	F_4
0.3	1.6	1.5	1.5	1.5
F_5	F_6	F_7	F_8	F_9
1.5	2	4	0.76	0.5
F_{10}	F_{11}	F_{12}	F_{13}	F_h
5.7	5.1	1	0.6	0.3
F_c				
3.1				

3. Results and Discussions of Proposed Antenna

3.1. Scattering Parameters

The fabricated antenna model is illustrated in Fig. 2 (a), and the measurement setup inside the anechoic chamber is shown in Fig. 2(b). The zoomed view of the device can be visualized in Fig. 2 (c). The results show that the device operates in a frequency range that extends from 30 – 50 GHz. This region of operation also correlates to a bandwidth percentage of 50%, i.e., 20 GHz. The return loss of the fabricated antenna measured is compared with the simulated return loss values and is depicted in Fig. 3. The measured findings observed were strongly in accord with predicted results, particularly over the entire band of projected frequency, providing a wideband response as illustrated in the figure.

3.2. Radiation Pattern

Here, the correlation between the simulated and the measured radiation characteristics of the intended antenna inside the anechoic chamber is presented. The proposed element in the X-Y plane at 33 GHz and 36 GHz exhibits the pattern as portrayed in Fig.4. The antenna exhibits a stable pattern at both frequencies. Fig. 4(a) depicts the pattern at 33 GHz, and Fig. 4(b) depicts the pattern radiated at 36 GHz. The designed antenna in the X-Y plane exhibits directional radiation characteristics. The spatial distribution of the antenna designed is plotted in the X-Z

plane and presented in Fig. 5. Fig. 5(a) depicts the patterns at 33 GHz, where it exhibits the directional pattern characteristics and nearly omnidirectional radiation patterns at 36 GHz as portrayed in Fig. 5(b). The measured results in each of the situations mentioned above exhibit a strong correlation with the simulated but with a small variation from the intended due to factors like fabrication and tolerance in the measurement setup.

3.3. Radiation Efficiency and Gain of Proposed Antenna

Fig. 6 (a) presents the similarity among the antenna gain simulated and measured. It offers an apex gain of 12.3 dBi at 36 GHz, as is evident in the figure mentioned above. Within the intended band, the radiation efficiency of the proposed antenna is greater than 89%, and the same is illustrated using the plot depicted in Fig. 6(b). The fabricated antenna was compared with cutting-edge antennas [27-29] listed in Table 2 to highlight and demonstrate its potential. The antenna design provides adequate performance parameters, with a measured gain of 12.3 dBi as the maximum value, a small size, and a wide bandwidth. However, the antennas described in the literature are either relatively bigger or have a narrow bandwidth and low gains.

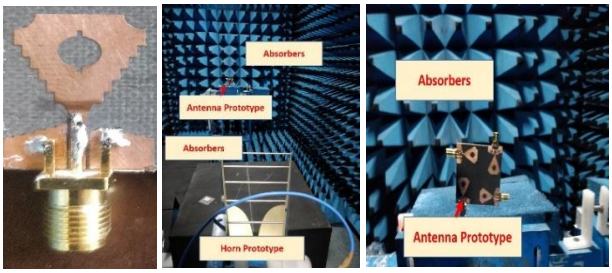

(a) (b) (c)

Fig. 2. Photograph of a) fabricated antenna, (b) the anechoic chamber measurement setup and (c) enlarged view of the antenna.

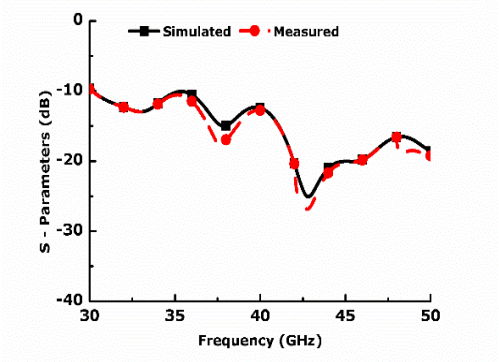

Fig. 3. Measured and simulated S-Parameters of the proposed antenna.

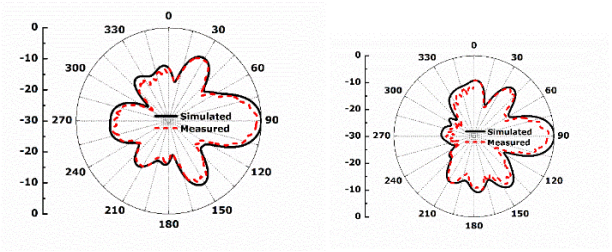

(a) (b)

Fig. 4. 2-D Polar plot of the antenna at (a) 33 GHz and (b) 36 GHz in the X-Y plane.

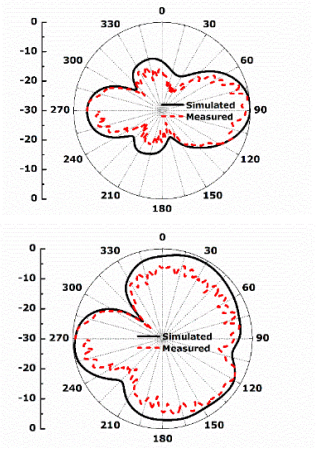

(a) (b)

Fig. 5. 2-D Polar plot of the antenna at (a) 33 GHz and (b) 36 GHz in the X-Z plane.

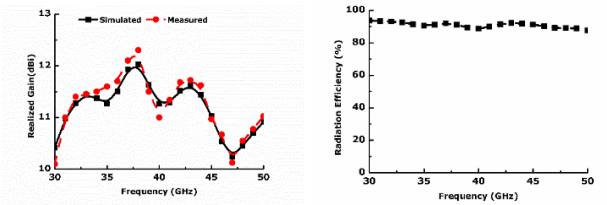

(a) (b)

Fig. 6. (a) Measured & Simulated gain (b) radiation efficiency of the suggested antenna.

Table 2: Comparison of the antenna performance to that of similar works currently in existence

Ref	Dimensions	Bandwidth (GHz)	Gain
[4]	5mm × 5mm	0.75 GHz	7 dBi
[14]	11 mm × 31mm	5 GHz	10 dBi
[26]	22 mm × 17 mm	4.5 GHz	8 dBi
[27]	2 mm × 2.5 mm	0.9 GHz	5.5 dBi
[28]	11 mm × 15 mm	3 GHz	3 dBi
[29]	15 mm × 15 mm	6.4 GHz	5.42 dBi
[35]	15 mm × 10 mm	3.8 GHz	5.83 dBi
This Work	**20** mm × **14** mm	**20** GHz	**12.3** dBi

4. Design Procedure of MIMO Antenna & Metasurface

The antenna proposed is converted to a 2X2 arranged four-

port MIMO configuration having the overall dimensions of 44 × 44 mm^2 (L_M × W_M) as depicted in Fig. 7. The front and rear view of the MIMO antenna configuration is illustrated in Fig. 7 (a) and 7 (b). The intended MIMO antenna is designed on RT Durioid 5880 substrate of a 1.575 mm thickness and permittivity ε_r = 2.2. After the MIMO design is completed, a metasurface design is done next. A metasurface of dimensions, as portrayed in Fig. 7 (c), is designed in the simulator. Initially, two circular rings are designed. One ring is obtained by subtracting R_2 (1.2 mm) from R_1 (1.3 mm), and the second ring is obtained by subtracting radius R_4 (0.7 mm) from R_3 (0.8 mm). A third circle of radius R_5 (0.35 mm) is made in the centre. After this, from the outer ring, a small patch of dimension 0.1 × 0.4 mm^2 is removed. This is followed by removing a patch of dimension 0.1 × 0.3 mm^2 from it. Finally, from the centre circle, two rectangular strips of dimension 0.7 × 0.1 mm^2 are removed to get a "+" shaped incision in the centre. The metamaterial unit cell is of dimension 3.8 × 3.8 mm^2 (L_C × W_C). The designed metasurface is replicated horizontally and vertically 14 times to get the final structure of the superstrate. Fig. 7 (d) shows the entire structure designed, which consists of the MIMO antenna arrangement together with the superstrate structure. The MIMO structure developed is illustrated in Fig. 8. Fig. 8(a) and (b) illustrate the front and rear portions of the fabricated MIMO antenna configuration, and Fig.8 (c) depicts the constructed structure along with the metamaterial superstrate. The proposed antenna in the MIMO configuration was simulated using a Full-wave EM simulator. To determine MIMO antenna transmission and reflection coefficient, the vector network analyzer of the Agilent PNA-X model was used. The anechoic chamber and its complete setup, illustrated in Fig. 9, were used to determine the radiation pattern in orthogonal planes. Various simulated and measured metrics of the 2 × 2 MIMO antenna are listed below.

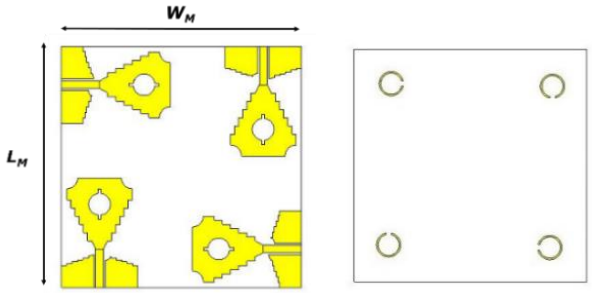

(a) (b)

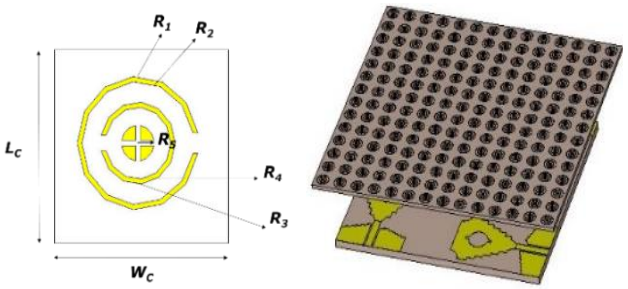

(c) (d)

Fig. 7. Proposed MIMMO antenna (a) front side of the MIMO configuration, (b) back side of the MIMO configuration, (c) designed metasurface and (d) complete device view.

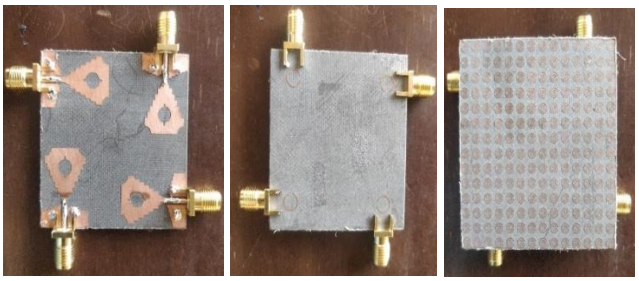

(a) (b) (c)

Fig. 8. The constructed MIMO antenna (a) front view (b) back view and (c) antenna structure with metasurface.

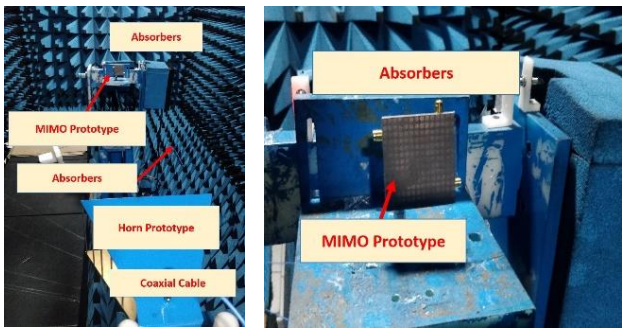

Fig. 9. The anechoic chamber measurement setup for radiation pattern of MIMO antenna (a) complete view and (b) zoomed view.

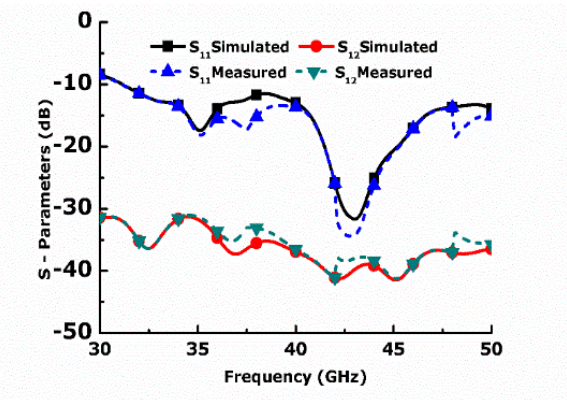

Fig. 10. MIMO antenna scattering parameters simulated and measured results.

5. Fabrication and Measurement of Proposed Antenna

5.1. Scattering Parameter

The measured and predicted properties of the MIMO configuration are compared and depicted. Due to the symmetry in the structure, the reflection and transmission scattering properties of all antennas remain almost the same; hence, the parameters of antennae 1 and 2 are only illustrated in the rest of the manuscript. From Fig. 10, it is noticed that the predicted and measured responses agree well, offering a measured impedance bandwidth of 20GHz that covers the frequency from 30-50 GHz. Additionally, It also offers a mutual coupling of < 31 dB within the mentioned band, which specifies good isolation between the antenna. The Scattering coefficients of the unit cell of the metasurface are designed and verified through Full-wave EM simulations with the setup depicted in Fig. 11 (a) and the obtained readings represented in Fig. 11 (b).

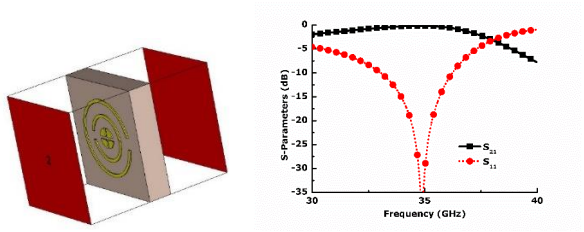

(a) (b)

Fig. 11. (a) Unit cell design and excitation (b) obtained S-parameter of the Unit cell readings.

5.2. Radiation Pattern

It is crucial to observe the radiation characteristics of an antenna as they give the device directional properties. Hence, the radiation characteristics measured inside the anechoic chamber are studied and validated upon comparison with the simulated patterns. The patterns radiated in the X-Y plane are depicted in Fig. 13. The 2-D radiated patterns at 33 GHz and 36 GHz are illustrated in Fig. 13 (a) and (b). The patterns in the X-Z plane of the proposed configuration are illustrated in Fig. 14. Fig. 14(a) & (b) illustrate the pattern radiated at 33 GHz and 36 GHz, respectively. A consistent pattern is radiation by the antenna at both frequencies and planes. In all the cases mentioned, the measured outcomes are in accord with the simulated results but with minor variation from the intended due to tolerance in the measurement setup and factors involved in fabrication.

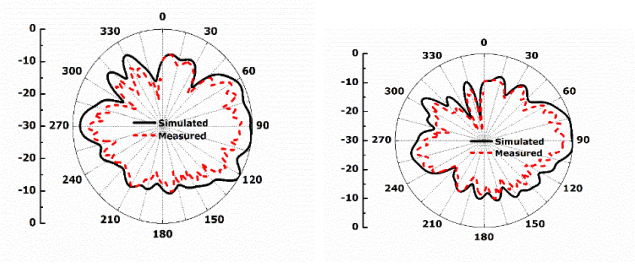

(a) (b)

Fig. 13. 2-D Polar plot of MIMO antenna at (a) 33 GHz and (b) 36 GHz in the X-Y plane.

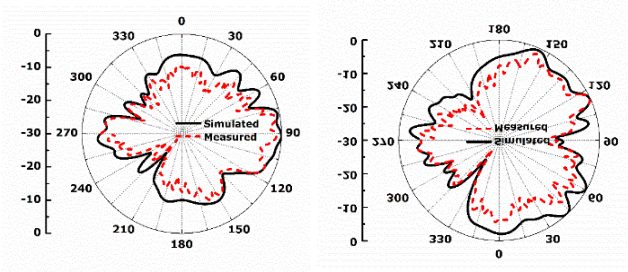

(a) (b)

Fig. 14. 2-D Polar plot of MIMO antenna at (a) 33 GHz and (b) 36 GHz in the X-Z plane.

5.3. The gain performance

Fig. 15 depicts the comparison of gain performance among the measured values with the simulated values with and without the superstrate of the proposed MIMO antenna. The gain performance without the superstrate material at 33 GHz and 36 GHz is nearly about 11 dBi and 11.5dBi respectively. Later this performance is enhanced around 13.6 dBi and 13.8 dBi at 33 GHz and 36 GHz respectively with the addition of the superstrate material. Thus, there is a gain enhancement of 3 dBi with the addition of superstrate.

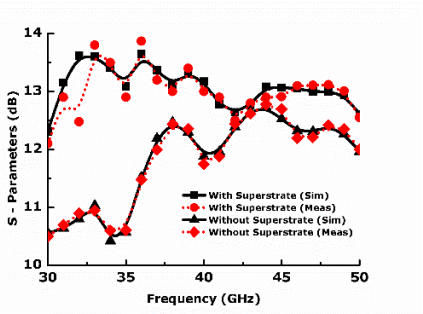

Fig. 15. Proposed MIMO antenna simulated and measured gain with and without superstrate.

6. MIMO Performance

Information about parameters such as the envelope correlation coefficient (ECC) and the gain of directives (DG) is of great significance in analyzing MIMO system performance. Hence, in the following subsections, the above-mentioned parameters for the intended MIMO configuration are discussed.

6.1. Envelop Correlation Coefficient

One of the most crucial variables for understanding the behaviour of MIMO antennas is the envelope correlation coefficient (ECC), which may be computed using (1). The ECC for neighbouring antennas element-1 and 2 for the proposed MIMO antenna were measured and simulated, as illustrated in Fig. 16. Using the calculations in [35], the radiation pattern or the S-parameter at the ports of the antenna can be used to assess the ECC of the MIMO antenna. The ECC of the proposed MIMO antenna, shown in Fig. 16, have a value < 0.0005 up to 32.5 GHz and < 0.0001 from 32.5 to 50 GHz, which is suitable for MIMO communication and lies within the acceptable range.

$$\rho_{eij} = \frac{|S_{ii}^{*}S_{ij} + S_{ji}^{*}S_{jj}|^2}{(1 - |S_{ii}|^2 - S_{ij}^2)(1 - |S_{ji}|^2 - S_{jj}^2)} \quad (1)$$

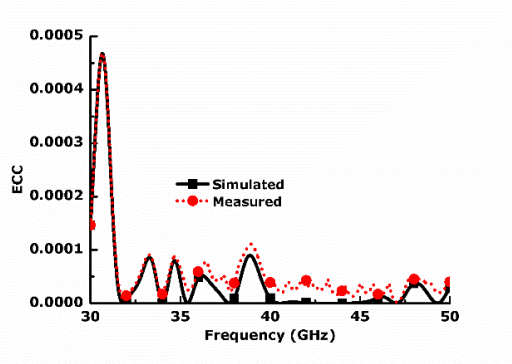

Fig. 16. ECC of the MIMO antenna.

6.2. Diversity Gain (DG)

Diversity gain (DG), an indicator of the transmission power loss resulting from using a MIMO antenna for the diversity scheme, can be determined using equation (2). Although a DG of 10 dB is the ideal value, in practice, an approximate value relatively close value to 10 dB is acceptable because of different losses. The suggested antenna's simulated and measured diversity gain between neighbouring antenna elements is shown in Fig. 17 to be more than 9.9995 dB over the functional range, suggesting that the antenna may find usage in diversity scheme applications.

$$DG = 10\sqrt{1 - |\rho_{eij}|^2} \quad (2)$$

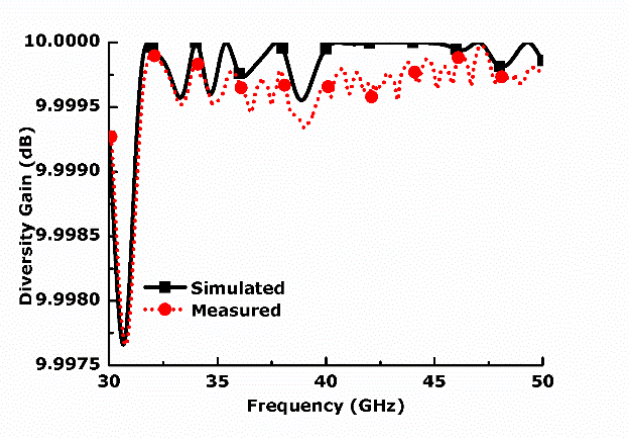

Fig. 17. Directive Gain of the MIMO antenna.

A comparison of the proposed MIMO antenna with the similar works that are already available in the literature is shown in Table 3. When compared to most published studies, the dimension of the suggested antenna is comparatively small. Comparing the proposed work to similar works, it has reduced mutual coupling, larger bandwidth, higher gain, and lower ECC.

Table 3: Comparison of the MIMO antenna performance to that of similar works currently in existence

Ref	Size	Ports	Bandwidth	Mutual Coupling	Gain	ECC
[8]	30mm × 35 mm	4	4.1 GHz	>-22 dB	8.3 dBi	0.5
[20]	11 mm × 31 mm	4	5 GHz	>-18 dB	10 dBi	0.04
[22]	28 mm × 30 mm	4	3 GHz	>-21 dB	6.2 dBi	0.05
[23]	12.5 mm × 12.5 mm	4	2 GHz	>-15 dB	6 dBi	0.02
[24]	60 mm × 100 mm	4	1.7 GHz	>-20 dB	9.8 dBi	-
[30]	115 mm × 65 mm	4	1.22 GHz	>-12 dB	4.85 dBi	0.1
This Work	44 mm × 44 mm	4	20 GHz	>-31 dB	13 dBi	0.0005

7. Conclusion

In this article, a compact wideband MIMO antenna for mmW applications is designed and verified experimentally for its properties. The initial antenna design offered a broad frequency range of 20 GHz and a peak gain of 12.3 dBi. The antenna design was then extended to design the 2 × 2 MIMO configuration having an overall size of 44 × 44 × 1.575 mm^3. A metamaterial superstrate was designed and placed above the MIMO antenna for improvement of gain. The proposed configuration of the MIMO antenna performs well in terms of metrics like isolation of value less than -31 dB, ECC of less than 0.0005 from 30 to 32.5 GHz and ECC of less than 0.0001 from 32.5 to 50 GHz. The device also obtains a high diversity gain greater than 9.99 dB from 32.5 to 50 GHz. Additionally, the suggested antenna has been compared to similar literary works, and it has been found to fare better than those works Hence, the intended antenna design is suitable for applications in the mmW band.

References

[1] Andrews, Jeffrey G., et al. "What will 5G be?." IEEE Journal on selected areas in communications 32.6 (2014): 1065-1082.

[2] Awan, Wahaj A., et al. "Stub loaded, low profile UWB antenna with independently controllable notch-bands." Microwave and Optical Technology Letters 61.11 (2019): 2447-2454.

[3] Hussain, Musa, et al. "A wideband antenna for V-band applications in 5G communications." 2021 International Bhurban Conference on Applied Sciences and Technologies (IBCAST). IEEE, 2021.

[4] Awan, Wahaj Abbas, Abir Zaidi, and Abdennaceur Baghdad. "Patch antenna with improved performance using DGS for 28GHz applications." 2019 International Conference on Wireless Technologies, Embedded and Intelligent Systems (WITS). IEEE, 2019.

[5] Hussain, Niamat, et al. "A broadband circularly polarized fabry-perot resonant antenna using a single-layered PRS for 5G MIMO applications." IEEE Access 7 (2019): 42897-42907.

[6] Naqvi, Aqeel Hussain, and Sungjoon Lim. "Review of recent phased arrays for millimeter-wave wireless communication." Sensors 18.10 (2018): 3194.

[7] Hussain, Musa, and Nabigha Nadeem. "A co-planar waveguide feed dual band antenna with frequency reconfigurability for WLAN and WiMax systems." 2019 International Conference on Electrical, Communication, and Computer Engineering (ICECCE). IEEE, 2019.

[8] Khalid, Mahnoor, et al. "4-Port MIMO antenna with defected ground structure for 5G millimeter wave applications." Electronics 9.1 (2020): 71.

[9] M. J. Al-Hasan, T. A. Denidni and A. R. Sebak, "Millimeter-Wave EBG-Based Aperture-Coupled Dielectric Resonator Antenna," in IEEE Transactions on Antennas and Propagation, vol. 61, no. 8, pp. 4354-4357, Aug. 2013, doi: 10.1109/TAP.2013.2262667.

[10] M. Akbari, S. Gupta, M. Farahani, A. R. Sebak and T. A. Denidni, "Gain Enhancement of Circularly Polarized Dielectric Resonator Antenna Based on FSS Superstrate for MMW Applications," in IEEE Transactions on Antennas and Propagation, vol. 64, no. 12, pp. 5542-5546, Dec. 2016, doi: 10.1109/TAP.2016.2623655.

[11] Mall, L., and R. B. Waterhouse. "Millimeter-wave proximity-coupled microstrip antenna on an extended hemispherical dielectric lens." IEEE Transactions on Antennas and Propagation 49.12 (2001): 1769-1772.

[12] Malik, Bilal Tariq, et al. "Antenna gain enhancement by using low-infill 3D-printed dielectric lens antennas." IEEE Access 7 (2019): 102467-102476.

[13] Attia, Hussein, M. Lamine Abdelghani, and Tayeb A. Denidni. "Wideband and high-gain millimeter-wave antenna based on FSS Fabry–Perot cavity." IEEE Transactions on Antennas and Propagation 65.10 (2017): 5589-5594.

[14] Wani, Zamir, Mahesh Pandurang Abegaonkar, and Shiban Kishen Koul. "A 28-GHz antenna for 5G MIMO applications." Progress In Electromagnetics Research Letters 78 (2018): 73-79.

[15] Asaadi, Muftah, Islam Afifi, and Abdel-Razik Sebak. "High gain and wideband high dense dielectric patch antenna using FSS superstrate for millimeter-wave applications." IEEE Access 6 (2018): 38243-38250.

[16] Akbari, Mohammad, et al. "Spatially decoupling of CP antennas based on FSS for 30-GHz MIMO systems." IEEE Access 5 (2017): 6527-6537.

[17] Murthy, Nimmagadda. "Improved isolation metamaterial inspired mm-Wave MIMO dielectric resonator antenna for 5G application." Progress In Electromagnetics Research C 100 (2020): 247-261.

[18] Farahani, Mohammadmahdi, et al. "Mutual coupling reduction in millimeter-wave MIMO antenna array using a metamaterial polarization-rotator wall." IEEE Antennas and Wireless Propagation Letters 16 (2017): 2324-2327.

[19] Jiang, Haixin, et al. "A symmetrical dual-beam bowtie antenna with gain enhancement using metamaterial for 5G MIMO applications." IEEE Photonics Journal 11.1 (2019): 1-9.

[20] Tu, Duong Thi Thanh, et al. "28/38 GHz dual-band MIMO antenna with low mutual coupling using novel round patch EBG cell for 5G applications." 2017 International Conference on Advanced Technologies for Communications (ATC). IEEE, 2017.

[21] Iqbal, Amjad, et al. "Electromagnetic bandgap backed millimeter-wave MIMO antenna for wearable applications." IEEE Access 7 (2019): 111135-111144.

[22] Khalid, Hassan, et al. "2X2 MIMO antenna with defected ground structure for mm-wave 5G applications." 2019 13th International Conference on Mathematics, Actuarial Science, Computer Science and Statistics (MACS). IEEE, 2019.

[23] Xing, Haoran, et al. "Efficient isolation of an MIMO antenna using defected ground structure." Electronics 9.8 (2020): 1265.

[24] Arabi, Omer, et al. "Compact Wideband MIMO

diversity antenna for mobile applications using multilayered structure." Electronics 9.8 (2020): 1307.

[25] Saad, Ayman Ayd R., and Hesham A. Mohamed. "Printed millimeter-wave MIMO-based slot antenna arrays for 5G networks." AEU-International Journal of Electronics and Communications 99 (2019): 59-69.

[26] Hakim, Mohammad Lutful, Mohammed Jashim Uddin, and MD Jiabul Hoque. "28/38 GHz dual-band microstrip patch antenna with DGS and stub-slot configurations and its 2× 2 MIMO antenna design for 5G wireless communication." 2020 IEEE Region 10 Symposium (TENSYMP). IEEE, 2020.

[27] Ohnimus, Florian, et al. "Design and Comparison of 24 GHz Patch Antennas on Glass Substrates for Compact Wireless Sensor Nodes." International Journal of Microwave Science and Technology 2010 (2010).

[28] Gu, Xiaoxiong, et al. "A multilayer organic package with 64 dual-polarized antennas for 28GHz 5G communication." 2017 IEEE MTT-S International Microwave Symposium (IMS). IEEE, 2017.

[29] Hussain, Niamat, et al. "Compact wideband patch antenna and its MIMO configuration for 28 GHz applications." AEU-International Journal of Electronics and Communications 132 (2021): 153612.

[30] Ikram, M., M. S. Sharawi, and Atif Shamim. "A novel very wideband integrated antenna system for 4G and 5G mm-wave applications." Microwave and Optical Technology Letters 59.12 (2017): 3082-3088.

[31] M. A. Shukoor and S. Dey, "Wideband Reconfigurable Multifunctional Absorber/Reflector With Bandpass/Bandstop Filtering and Band-Notch Absorption for RCS and EMI Shielding," IEEE Transactions on Electromagnetic Compatibility, doi: 10.1109/TEMC.2023.3306019.

[32] M. A. Shukoor, S. Dey and S. K. Koul, "A Novel Interdigital Capacitances (IDCs) Based Linear-Cross Reflective Type Polarization Converter for X- and Ku-Band Applications," 2021 IEEE Indian Conference on Antennas and Propagation (InCAP)", Jaipur, Rajasthan, India, pp. 629-632, 2021.

[33] M. A. Shukoor and S. Dey, "A novel broadband linear-cross and linear-circular reflective polarizer based on interdigital capacitance loaded dipole for radar cross-section applications," International Journal of RF and Microwave

[34] M. A. Shukoor and S. Dey, "Novel broadband angular stable linear-circular and linear-cross polarizer based on inductive grid loaded H-dipole in both reflection and transmission modes," International Journal of RF and Microwave Computer-Aided Engineering", vol. 32, no. 8, pp. 23226, 2021.

[35] M. A. Shukoor and S. Dey, "Compact, broadband, wide angular stable circuit analogue absorber at sub-6 GHz for radar cross section reduction", Microwave and Optical Technology Letters, vol. 63, no. 12, pp. 2938-2943, 2021.